Green Chemistry

PAPER

View Article Online
View Journal | View Issue

Cite this: *Green Chem.*, 2020, **22**, 7871

Plasma electrolysis of cellulose in polar aprotic solvents for production of levoglucosenone†

Lusi A,[a] Harish Radhakrishnan,[a] Haiyang Hu,[b] Hui Hu[b] and Xianglan Bai *[a]

Received 18th August 2020,
Accepted 21st October 2020

DOI: 10.1039/d0gc02813d

rsc.li/greenchem

In this study, we demonstrated the use of plasma electrolysis as a low-energy, efficient method of producing biobased chemicals from cellulose. We used high-voltage alternative current electricity as the plasma source in polar aprotic solvents to achieve complete liquefaction of cellulose without the use of external heating. A levoglucosenone yield of 43% was obtained after 15 min of conversion in γ-valerolactone using a voltage of 6 kV and frequency of 6 kHz, and a 38% yield was obtained within 3 min in sulfolane using a voltage of 4 kV (or 40% after treating for 7 min with the voltage of 3.5 kV). Compared to conventional liquefaction in the same solvents, plasma electrolysis could produce much greater LGO yields using significantly less energy. In this study, the plasma electrolysis of cellulose in γ-valerolactone was able to increase the levoglucosenone yield by 154% while using only 28% of the energy consumed during conventional thermal-based conversion of cellulose in the same solvent for producing its maximum yield of 17%. When the same conversions were performed in sulfolane, a 28% higher levoglucosenone yield was produced while requiring only 3% of the energy consumed during the respective thermal-based conversion of cellulose to obtain its maximum yield of 31.2%. The study also revealed that the plasma electrolysis of cellulose proceeds through novel radical-based mechanisms involving *in situ*-generated hydrogen radicals, by which cellulose depolymerizes and dehydrates much more efficiently than it does during conventional liquefaction. During the plasma electrolysis process, cellulose conversion was significantly enhanced by synergistic effects between Joule heating and plasma chemistry.

1. Introduction

Biobased chemical production is a highly attractive method of biomass valorization because chemicals usually have higher economic value than biofuels.[1–4] Through deconstructing and upgrading, a range of chemicals can be produced, including petroleum-derivable chemicals and chemicals with unique structures and properties that are difficult to produce from petroleum feedstocks.[5] Despite these advantages, biobased chemicals are currently underdeveloped, and selectively converting biomass in a cost-competitive way remains a significant challenge. Primary complications, such as improving the selectivity of the reaction to enhance the product yield, increasing the reaction rate, and lowering the production energy, have yet to be addressed. Developing low-energy, low-cost technologies to enable selective and robust conversions will greatly help in the economical production of the biobased chemicals.

Non-thermal plasma (NTP) is emerging as a novel technology to convert biomass. Plasma, known as the fourth state of matter in the universe, is composed of electrons, ions, free radicals, molecules, and atoms. NTP is usually generated by applying a high electric field to gases to cause electron ionization and bond dissociations.[6] Since a chemically rich environment is created under mild conditions, NTP enabled reactions are usually hard to initiate using conventional technologies with the same reaction conditions. So far, NTP has been explored as a green alternative technology in biomass pretreatment, biomass decomposition, and catalytic upgrading.[7–11] For example, the plasma treatment was able to delignify biomass and decrystalize cellulose at near room temperature.[12–19] Coupling NTP with conventional pyrolysis or catalytic pyrolysis was able to improve bio-oil quality and/or reduce catalyst deactivation.[10,20–22] In a recent study, we also explored plasma-assisted pyrolysis to enhance cellulose conversion to levoglucosan (LG) without using any catalysts or solvents.[23] While previous studies have explored the use of NTP discharges for gas-phase reactions, the plasma electrolysis in solutions was rarely explored.[24–26] Tang *et al.* previously investigated the plasma electrolysis of biomass in a co-solvent of polyethylene glycol and glycerol, reporting a reduced reaction time and/or lower

[a]*Department of Mechanical Engineering, Iowa State University, Ames, IA 50011, USA. E-mail: bxl9801@iastate.edu*
[b]*Department of Aerospace Engineering, Iowa State University, Ames, IA 50011, USA*
†Electronic supplementary information (ESI) available. See DOI: 10.1039/d0gc02813d

energy input compared to conventional liquefaction of biomass.[27–30] They also reported that the crude bio-oil produced from the plasma electrolysis process is similar to the conventionally liquified bio-oil.

In this study, for the first time, we demonstrate the use of plasma electrolysis of cellulose in polar aprotic solvents as a low-energy, efficient method of producing levoglucosenone (LGO) and other oxygenated chemicals. LGO is a highly attractive biobased molecule. It is a precursor chemical that has wide applications in pharmaceuticals, the synthesis of biobased solvents, and polymers.[31–35] Previously, LGO was mostly produced during catalytic pyrolysis of biomass. For example, Ye *et al.* reported an LGO yield of 14.7% by catalytically pyrolyzing cellulose using activated carbon.[36] Zhang *et al.* reported an LGO yield of 16.1% from pyrolysis of cellulose catalyzed by solid phosphoric acid.[37] Kudo *et al.* conducted the reforming of cellulose pyrolysis vapor using ionic liquid as both a solvent and catalyst to produce up to a 22% yield of LGO.[38] Disadvantages of LGO production based on catalytic pyrolysis include high reaction temperatures (up to 450 °C), low product yields, the need for pretreating biomass, as well as the requirement for catalyst recovery.

On the other hand, LGO could also be produced through conversions in polar aprotic solvents using common acid catalysts.[31,32] Unlike polar protic solvents, such as water and alcohols, polar aprotic solvents do not hydrolyze cellulose. Compared to using water as the solvent, polar aprotic solvents can significantly promote acid-catalyzed reactions by affecting the stability of the acidic proton relative to protonated transition states.[39,40] Previously, Kawamoto *et al.* converted cellulose at 200 °C in a sulfolane solution using sulfuric acid as the catalyst.[41] The pyrolytic vapors were then condensed downstream to obtain an LGO yield of 30.3% under atmospheric pressure, or a yield of 42.2% using a vacuum recovery. In another study, Cao *et al.* converted cellulose at 210 °C in tetrahydrofuran solution with sulfuric acid using an autoclave batch reactor to produce up to 51% yield of LGO.[31] Although higher LGO yields could be obtained by converting cellulose in polar aprotic solvents, solvent-phase conversions usually have lower reaction rates and increased reaction times compared to gas-phase conversions due to lower operating temperatures.

In this study, the plasma electrolysis of cellulose was performed by applying a high-voltage alternative current (AC) in γ-valerolactone (GVL) or sulfolane. Both the solvents were previously studied in biomass conversions where they showed better performances than some of other polar aprotic solvents due to their high polarities.[39–44] GVL is also a biomass-derivable green solvent.[45] Cellulose was also converted in the corresponding solvents using a conventional thermal heating to compare the plasma electrolysis and the traditional solvent-based conversion in terms of product distribution and energy consumption. Subsequently, the underlying phenomena and reaction mechanisms relevant to the plasma electrolysis of cellulose were investigated.

2. Materials and methods

2.1 Materials

Microcrystalline cellulose, GVL (≥99%), sulfolane (99%), furfural (FF), 5-hydroxylmethyl furan (HMF), and 1,4:3,6-dianhydro-α-D-glucopyranose (DGP) were purchased from Sigma Aldrich. Sulfuric acid (99.6 wt%) and glucose were from Fisher Scientific, and levoglucosenone (LGO, 99.9%) and levoglucosan (LG, 99.9%) were purchased from Carbosynth Ltd. Levulinic acid (LA) was purchased from Acros Organics. *N-tert*-Butyl-α-phenylnitrone (PBN) was purchased from TCI America, and 5,5-dimethyl-1-pyrroline-*N*-oxide (DMPO) was from Matrix Scientific. Deionized water with the electric resistance of 18.2 MΩ was available on site.

2.2 Cellulose conversions

The plasma electrolysis of cellulose was performed using a 30 mL three-neck round-bottom flask containing 8 mL of GVL or sulfolane and varied amounts of sulfuric acid or different cellulose loadings. Two tungsten rods were inserted into the solvent at room temperature to act as a high-voltage electrode and a ground electrode, respectively. The high-voltage electrode was connected to a high voltage AC power supply (Suman Company, CTP-2000 K) as a plasma generator. The frequency of the AC power was fixed at 6 kHz and varied voltages were applied. The electric current–voltage waveform was monitored by an oscilloscope (Tektronix DPO3054).

The electric current and voltage were also measured using a high response current probe (Pearson Electronics, Inc., Pearson 2877) and a high voltage probe (*i.e.*, P6015A from Tektronix). During the conversion, the flask was insulated, and a stir bar was placed inside the reactor for agitation. The solvent temperature was measured by a K-type thermocouple and thermometer (Oakton TEMP 100). When the reactor temperature had to be controlled, the flask was placed inside a water bath maintained at 50 °C. When spin trapping agents were tested, 25 mg of PBN or DMPO was added to GVL. For the plasma electrolysis of model compounds, 100 mg of glucose or LG was converted in GVL and acid.

For thermal-based conversion, a 40 mL reaction vessel containing cellulose and a solution was tightly wrapped with heating tape and insulated by glass wool. The heating tape and a K-type thermocouple were connected to a PID controller (Digi-Sense, Single-zone temperature controller). The power of the heater was 160 W. The reaction time for thermal-based conversion was counted from the start of the heating process.

2.3 Product characterizations

An Agilent 7890B Gas Chromatograph (GC) equipped with Mass Spectrometer (MS) and Flame Ionization Detector (FID) with two ZB-1701 capillary columns (60 m × 0.250 mm and 0.250 μm film thickness) were used to analyze the liquid products. Initially, the GC oven temperature was held at 40 °C for 3 min and then heated to 280 °C at a heating ramp of 4 °C min^{-1}. Finally, the oven was held at this temperature for an additional 4 min. In the GC, the inlet temperature was 280 °C.

Helium was the carrier gas with the column flow rate of 1 mL min^{-1} and the split ratio of 20 : 1 at the GC inlet. The FID detector temperature was 280 °C with hydrogen and airflow in 5 mL min^{-1}. The composition of the liquid products was identified with MS based on NIST liberary and quantified by FID. Calibration curves in the GC were created by injecting LGO, FF, DGF, LA, HMF and LG dissolved in methanol at different concentrations and measuring the peak areas in their corresponding GC-FID chromatograms. For each compound, a five-point calibration curve with a regression coefficient higher than 0.99 was obtained. The similar GC analysis method was employed in previous studies to analyze biomass-derived products.[39,43] In this study, carbon mole-based product yields were calculated using the following equation:

$$\text{Product yield(C\%)} = \frac{\text{Carbon mole in product}}{\text{Carbon mole in feedstock}}$$

The liquid products were also analyzed using Gel Filtration Chromatography (GFC). GFC analysis was conducted with a Dionex Ultimate 3000 series HPLC system using water as the eluent. The liquid fraction from the plasma electrolysis was diluted using a 10 times volume of deionized water. Water at 25 °C and a flow rate of 1.0 mL min^{-1} was used as the mobile phase in two PL-aquagel-OH-20 5 μm columns connected in series and a refractive index detector was used. The identification of glucose was based on the retention time of its standard chemical in the GFC chromatogram.

The electrical resistance of the solution was measured using a multimeter (Greenlee DM-100). The acidity of the liquids were also measured using a pH meter (Mettler Toledo SevenMulti pH meter) after diluting the liquid using DI water 10 times.

The Optical Emission Spectroscopy (OES) was performed using an Ocean Optics USB4000 spectrometer on the absorbance function and a DT-Mini-2 UV-Vis light source. The spectrometer wavelength was calibrated with an HG-1 Mercury Argon calibration source.

Electron Paramagnetic Resonance (EPR) spectra were recorded on a Bruker ELEXYS E580 FT-EPR spectrometer at the X-band microwave frequency (9.83 GHz) with a magnetic field modulation of 100 kHz at room temperature.

3. Results and discussion

3.1 Cellulose conversion in GVL

3.1.1 Effect of acid concentration during the plasma electrolysis in GVL. Prior to performing the plasma electrolysis of cellulose, the voltage of the plasma generator was gradually increased to determine the minimum voltage required for causing a dielectric breakdown in the solution (*i.e.*, the breakdown voltage). The dielectric breakdown can be determined by monitoring the electric current–voltage waveform during the reaction. When the applied voltage is above the breakdown voltage, plasma ionization and electron emissions inside the solvent cause a transition from dielectric substance to conductive substance. In the GVL solutions with an acid concentration in the range of 3.5 mM to 14 mM, the voltages above 5 kV could cause the breakdown. However, the breakdown was not observed in pure GVL even after the voltage was increased to 7 kV. During the plasma electrolysis in the acidic GVL solutions, small gas bubbles were initially observed near the high-voltage electrode. Subsequently, flow motion was generated inside the solution in the reactor. Although external heating was absent, the increase of the solution temperature was observed during the plasma electrolysis.

The effects of acid concentration on the plasma electrolysis of cellulose were investigated by applying an AC voltage, with a voltage of 6 kV and a frequency of 6 kHz to GVL solutions containing different amounts of acid. The profiles of the solution temperature are given in Fig. 1(a). The increase in solution temperature depended on the acid concentration in the solvent. Without acid, the solvent temperature only increased by 10 °C after a 10 min reaction (no plasma formation at this condition). In comparison, the solution temperature increased much faster when acid was present. With 3.5 mM of acid, the solution temperature increased to 154 °C during a 7 min reaction. With 7 mM of acid, it only took 3.5 min to reach a similar temperature. However, the temperature did not increase faster with 10 mM of acid; the increase instead slowed down with 14 mM of acid. Interestingly, the solution temperatures all became stabilized at around 160 °C for different acid concentrations at extended reaction times.

Since the plasma electrolysis was not established with pure GVL under the applied AC voltage conditions, only GVL solutions with acid were investigated for cellulose conversions. During the plasma electrolysis, cellulose could completely liquefy after 5 to 7 min reactions with different acid concentrations. The major monomer products detected by GC/MS include LGO, DGP, FF, and LA. Other minor products were 1,3-butanediol, 2-butene, and 3-furan carboxylic acid methyl ester. Additionally, glucose was also detected by GFC. However, LG and HMF, which are the common products of cellulose during conventional conversions in polar aprotic solvents,[31,41,43] were not found in the liquid products based on the GC analysis (Fig. S1†). The yields of LGO, DGP, FF, and LA were quantified in Fig. 1(b)–(e) to compare the different acid concentrations and reaction times. LGO yield could reach 28–30% after only 5 min depending on the acid concentration. The maximum LGO yield was 38.6% with 3.5 mM of acid and 43.3% with 7 mM of acid, both achieved after a 15 min reaction. With these acid concentrations, the LGO was relatively stable in the solutions with prolonged reaction times. The rate for LGO formation became higher with higher acid concentrations. However, higher acid concentrations negatively affected LGO stability in the solution. The LGO yield reached 39.3% with 10.5 mM of acid after a 7.5 min reaction and then leveled off, and it decreased sharply with 14 mM of acid after reaching the maximum yield after a 5 min reaction. DGP, a polycyclic anhydrosugar, was the second most abundant monomer. Its yield was higher with lower acid concentrations in the solution, and the maximum yield of 15.2% was observed with 3.5 mM of

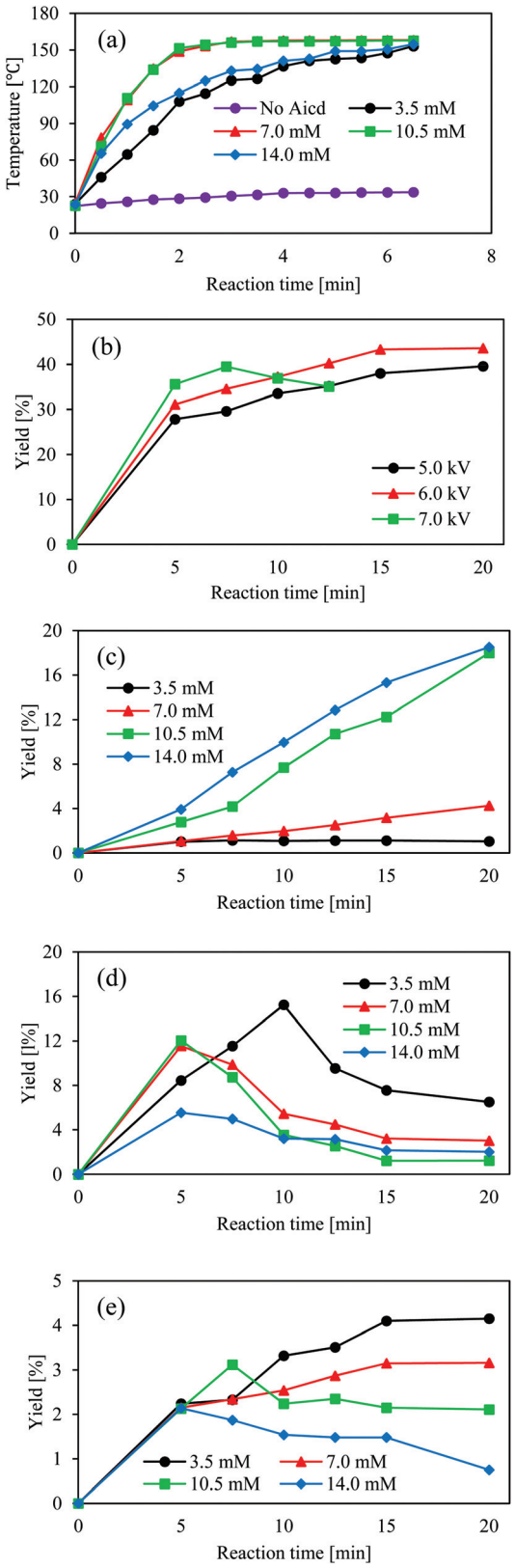

Fig. 1 Effect of acid concentration on (a) GVL solution temperature and product yields of (b) LGO, (c) FF, (d) DGF and (e) LA. Reaction conditions: 1.2 wt% cellulose, 8 mL GVL, V = 6 kV, f = 6 kHz. The same cellulose loading and solvent volume was used in the following tables and figures unless specified.

acid after 10 min reaction. On the other hand, FF formation was promoted by both higher acid concentration and increased reaction time. With 14 mM of acid, an 18.5% yield of furfural was obtained after 20 min. LA yield was in the range of 1–4% for conversions with different acid concentrations. While glucose was not quantified, it usually appeared in the early stage of the conversion and then degraded. From the GFC chromatograms given in Fig. S2,† the glucose peak was observed after a 5 min reaction in GVL with 7 mM of acid (the yield is estimated to be 6% based on the peak area in the GFC chromatogram), but the peak was no longer visible after a 10 min reaction.

3.1.2. Effect of electric voltage during the plasma electrolysis in GVL. Since the optimum acid concentration for LGO production was 7 mM, the effect of AC electric voltage was investigated by applying the voltages of 5 kV, 6 kV, or 7 kV (with a fixed frequency of 6 kHz) to convert the cellulose in the GVL with 7 mM of acid. As shown in Fig. 2(a), the solvent temperatures increased faster with higher voltages. With 7 kV voltage, the solution temperature reached 160 °C in 2.5 min and then stabilized with increasing reaction time. With 5 kV voltage, the solution temperature increased at a much slower rate, touching 140 °C only after a 20 min conversion. The product distributions are given in Fig. 2(b)–(e) to compare the conversions with different voltages. The maximum LGO yield was 39.5% for both the conversions with 7 kV and 5 kV voltage, which is lower than the 43.3% yield from the conversion at 6 kV voltage. It took 20 min to reach the maximum yield with 5 kV, while it only took 7.5 min with 7 kV. Increasing the voltage promoted the higher yields of FF, LA, and DGP and increased the reaction rates. However, applying a higher voltage also increased the product instability in the solutions for all monomers except FF.

3.1.3 Effect of cellulose loading during the plasma electrolysis in GVL. The effects of cellulose loading on LGO yield were investigated by applying the optimal voltage of 6 kV to the cellulose in GVL with 7 mM of acid. As given in Table 1, the maximum LGO yield and the corresponding reaction time depended on cellulose loading. The maximum LGO yield decreased from 43.3% with 1.2% cellulose to 37.5% with 2.4% cellulose, and 24.0% with 6.0% cellulose loading conditions. On the other hand, higher cellulose loading promoted higher yields of FF and DGP. The total yields of the four main monomers were 52.9%, 55.1%, and 44.1%, respectively, for the cellulose loadings of 1.2%, 2.4%, and 6.0%.

3.1.4. Cellulose conversion in GVL by thermal heating. A reactor containing cellulose, GVL with 7 mM of acid, was externally heated to 160 °C or 207 °C to compare the results of the plasma electrolysis with conventional liquefaction by thermal heating in Table 2. For a fair comparison, the same amount of cellulose was converted in the same volume of the solvent using both plasma electrolysis and the thermal method. The maximum LGO yields based on the thermal method were 10.6% at 160 °C after a 26 min reaction, and 17% at 207 °C after a 16 min reaction. In both the cases, solid residues were also produced by cellulose conversion. In a previous study,

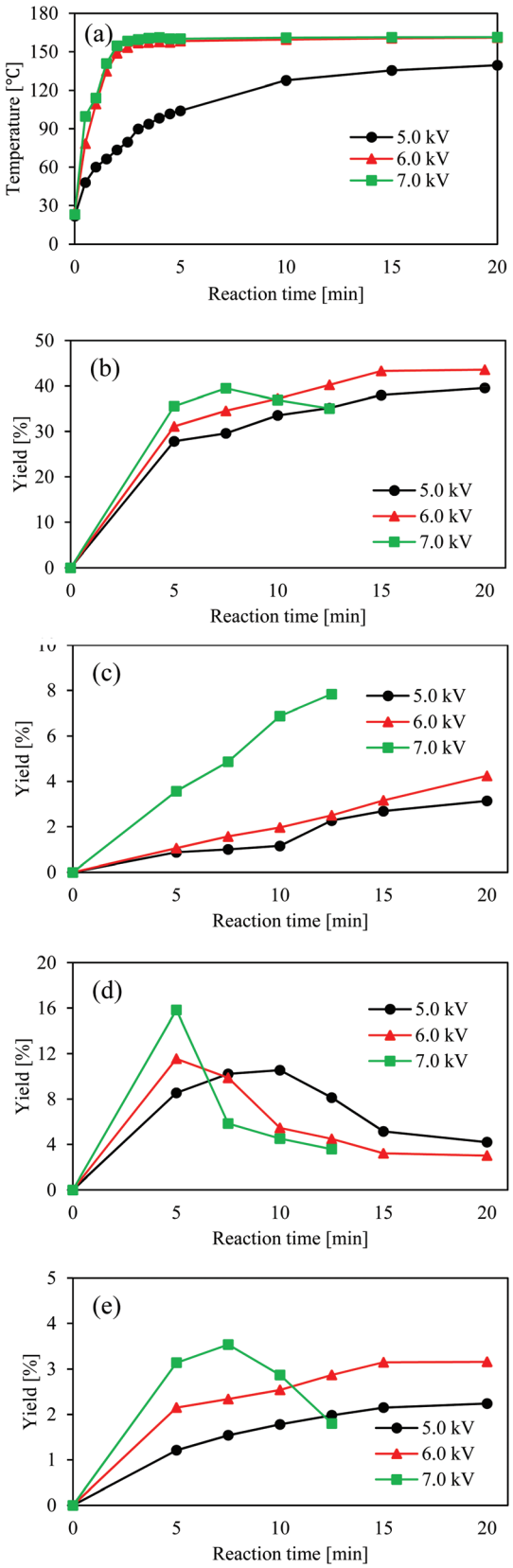

Fig. 2 Effect of AC voltage on (a) GVL solution temperature and product yields of (b) LGO, (c) FF, (d) DGF and (e) LA. Reaction conditions: 7 mM acid, f = 6 kHz.

Table 1 Effect of cellulose loading in GVL on product distribution (reaction conditions: V = 6 kV, f = 6 kHz, 7 mM acid)

		Yield [mol%]			
Cellulose [wt%]	Time [min]	FF	LGO	LA	DGP
1.2	15	3.2	43.3	3.2	3.2
	20	4.2	43.6	3.2	3.0
2.4	12.5	6.6	37.5	4.1	7.5
	15	8.6	35.5	3.4	6.6
6.0	10	7.9	24.0	3.7	8.5
	15	9.5	20.5	3.1	6.5

Cao *et al.* converted 1% cellulose in GVL and sulfuric acid using an autoclave batch reactor to report a maximum LGO yield of 15% at the reaction temperature of 170 °C with 5 mM of acid after a reaction that lasted for more than 80 min, and 12% at 190 °C with 7.5 mM of acid after more than 40 min.[31] As given, the LGO yields obtained using conventional thermal methods are all far below the product yield achieved by the plasma electrolysis in the same solvent.

3.2. Cellulose conversion in sulfolane

3.2.1. The plasma electrolysis of cellulose in sulfolane. The plasma electrolysis of cellulose in sulfolane was also investigated using sulfuric acid concentration ranging from 1.1 to 7 mM. In comparison to GVL, lower breakdown voltages could be applied (3.5 kV or above) in sulfolane. The profiles of the solution temperature during the plasma electrolysis with an applied voltage of 4 kV and a frequency of 6 kHz are given in Fig. 3(a) for different acid concentrations in the solution. The solution temperature increased at faster rates with increasing acid concentrations until 2.3 mM, reaching 123 °C after 3 min and 164 °C after 10 min. However, further increasing the acid concentration to 4.4 or 7 mM resulted in a slower rate of increase and lower temperatures of the solutions.

The corresponding product distributions are given in Fig. 3(b)–(e). Despite the application of a lower voltage, the reaction rate of cellulose was much faster with sulfolane solutions than with GVL solutions. For the sulfolane with 2.3 mM of acid, the maximum LGO yield of 37.9% was obtained after just 3 min. Similarly to what was previously observed during cellulose conversion in GVL, higher acid concentrations caused the reduced maximum yield of LGO but increased FF yields. DGP was also the second most abundant monomer, and it always reached the maximum yields earlier than LGO did in the same solutions. While it was not observed during the plasma electrolysis in GVL, LG was among the products in sulfolane. However, its yields were not significant regardless of the acid concentration in the solution. With 2.3 mM acid, its maximum yield was 1.1% achieved after a 7 min reaction. The lowest acid concentration of 1.1 mM not only increased the solution temperature at a slower rate, but also resulted in the lowest monomer yields. Notably, DGP, rather than LGO, was the primary monomer in the solution with this acid concentration.

Table 2 Comparison of product distributions during cellulose conversion based on plasma electrolysis and the thermal method

			Yield [mol%]					
Method	Sulfuric acid [mM]	Time[a] [min]	LGO	FF	LA	DGP	LG	Solid residue[b]
GVL, plasma electrolysis[c]	7	15	43.3	3.2	3.2	3.2	0.0	0.0
GVL, thermal 160 °C	7	26	10.6	2.2	2.0	2.3	0.0	21.1
GVL, thermal 207 °C	7	16	17.0	10.4	0.7	5.2	3.1	19.7
Sulfolane, plasma electrolysis[d]	2.3	7	37.9	0.4	1.1	5.1	0.7	0.0
Sulfolane, plasma electrolysis[e]	2.3	3	39.8	1.0	1.3	3.2	1.5	0.0
Sulfolane, thermal 160 °C	2.3	50	14.9	0.1	0.0	0.3	0.5	15.8
Sulfolane, thermal 207 °C	2.3	20	0.9	31.2	1.2	1.6	2.5	9.8

[a] The optimum reaction times for maximum LGO yields. [b] The solid residue yields are based on wt%. [c] V = 6 kV, f = 6 kHz. [d] V = 3.5 kV, f = 6 kHz. [e] V = 4 kV, f = 6 kHz.

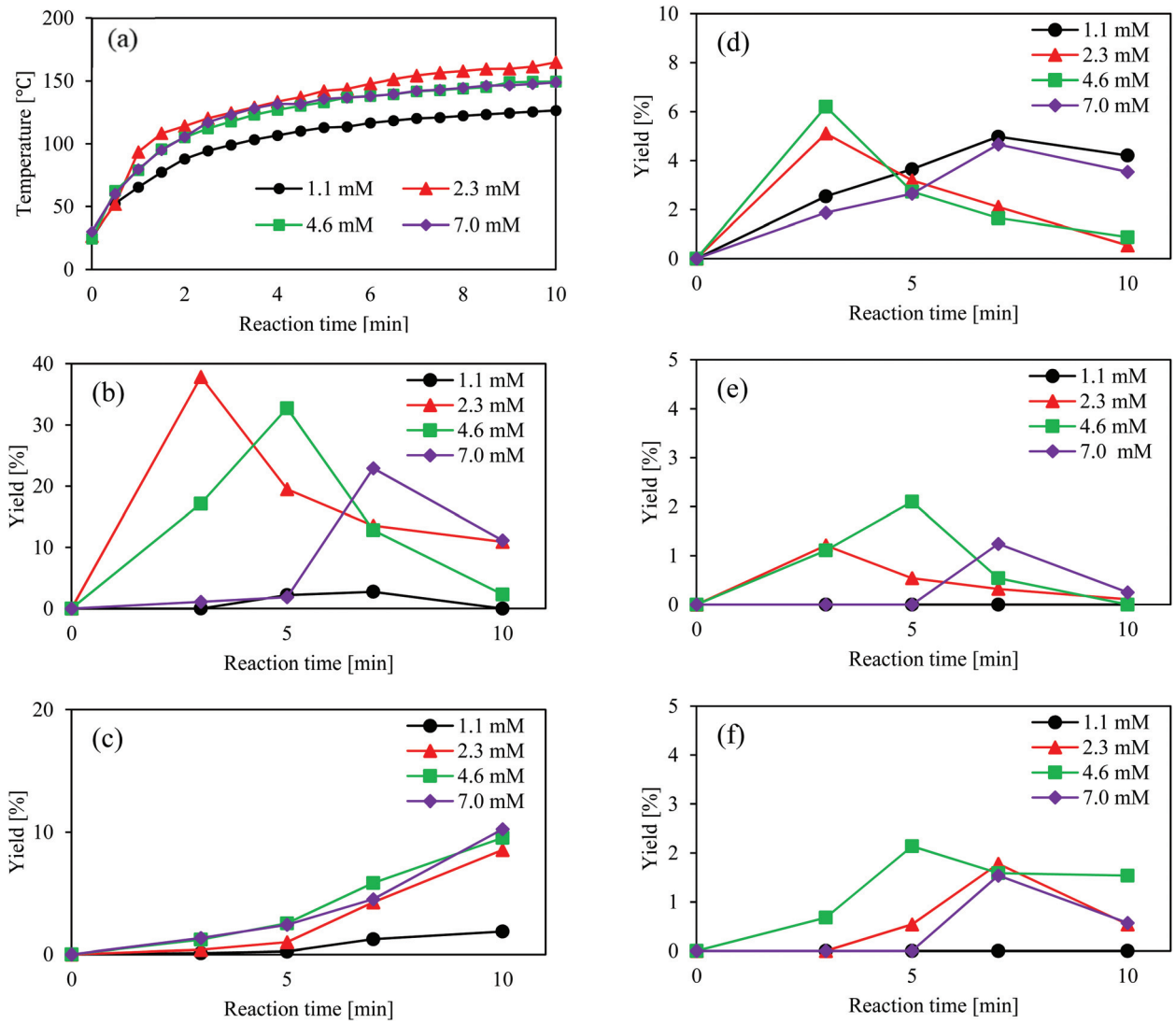

Fig. 3 Effect of acid concentration on (a) sulfolane solution temperature and product yields of (b) LGO, (c) FF, (d) DGF, (e) LA and (f) LG. Reaction conditions: V = 4 kV, f = 6 kHz.

Since it was the optimal acid concentration, cellulose in sulfolane with 2.3 mM of acid was also converted by applying a lower voltage of 3.5 kV. As a result, the maximum LGO yield increased to 39.8% (Fig. S3†). While the optimum reaction time increased to 7 min, LGO was much more stable in the solution with this lower voltage.

3.2.2. Conventional thermal conversion of cellulose in sulfolane. Cellulose conversion in sulfolane with 2.3 mM of acid was performed at 160 °C and 207 °C using the thermal method. The results are also included in Table 2 to compare it with the plasma electrolysis of cellulose in the same solution. The maximum LGO yields were 14.9% after a 50 min reaction at 160 °C, and 31.2% after reacting at 207 °C for 20 min. Thus, while both used a sulfolane solvent, higher LGO yields were obtained by using the plasma electrolysis instead of the thermal method.

3.3. Comparison of energy consumptions

Fig. 4 shows the profiles of input power during the plasma electrolysis of cellulose in GVL or in sulfolane for their respective optimal acid concentrations for producing higher LGO yields. In both the solutions, the power consumption during the plasma electrolysis decreased as the reaction proceeded, which is likely due to the dielectric breakdown and the decreased solution resistance for the passing electrical current. The input power was much lower in the sulfolane solution than it was in the GVL solution. The total energy consumptions during plasma electrolysis were calculated based on the power profiles shown in Fig. 4 for their respective solutions and the corresponding reactions times. As a result, the energy consumption was 0.012 kW h for producing 43.3% LGO in GVL, and 0.002 kW h for producing 39.8% LGO in sulfolane.

The energy consumptions during the thermal-based conversions of cellulose in the GVL and sulfolane solutions were also calculated based on the heater power and the reaction conditions listed in Table 2 for their respective maximum LGO yields. To produce an LGO yield of 17% in the GVL solution at 207 °C, it required 0.043 kW h thermal energy. Thus, the comparison shows that the plasma electrolysis of cellulose in GVL was able to increase the maximum LGO yield by 154% using only 28% of the energy used during the thermal conversion for producing its 17% yield. On the other hand, the energy consumption during the cellulose conversion in sulfolane at 207 °C was 0.053 kW h for producing an LGO yield of 31.2%. Therefore, a 28% higher LGO yield could be obtained by performing the plasma electrolysis in sulfolane, while using only 3% of the energy used to produce the 31.2% yield from the thermal-based conversion in the same solvent.

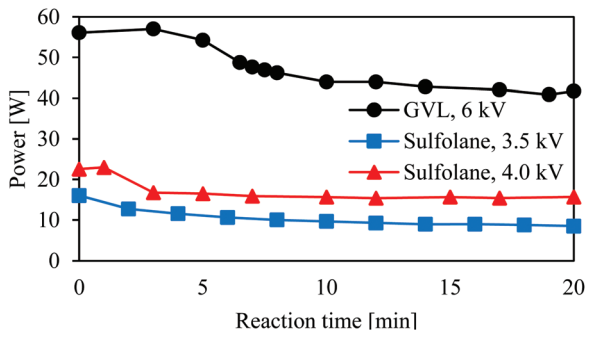

Fig. 4 Power inputs during plasma electrolysis of cellulose in GVL with 7 mM acid, and in sulfolane with 2.3 mM acid. The frequency is 6 kHz in all three cases.

In addition to comparing the product yields and energy consumptions, solvent degradations during the reactions were also investigated in this study. The degradation rates of GVL calculated using the mass differences of the solvent before and after the reactions were 0.0017 wt% per min during plasma electrolysis, and 0.0018 wt% per min during the thermal-based conversion at 207 °C. In comparison, sulfolane was stable during both plasma electrolysis and the thermal-based conversions.

3.4 Elucidating phenomena and mechanisms for plasma electrolysis of cellulose

3.4.1. Dielectric breakdown and the solution temperature. The plasma electrolysis demonstrated in this work outperformed the conventional liquefaction in the solvents by achieving complete liquefaction of cellulose and producing much greater LGO yields using significantly lesser energy inputs. The mechanism for the *in situ* increase of the solution temperature and its role during the plasma electrolysis of cellulose are discussed below to understand the underlying phenomena.

Both GVL and sulfolane are dielectric solvents that do not contain free charge carriers. When the applied AC voltage is below the breakdown threshold, dielectric heating is the primary mechanism that causes the solvent temperature to increase. Dielectric heating is caused by the twisting and vibrating of dielectric molecules placed under an AC electric field. The small temperature increase observed with cellulose in pure GVL described above in Fig. 1 was due to dielectric heating since the breakdown was not achieved under the given voltage condition.

Adding acid can introduce charged carriers in the solvent, thus increasing solution conductivity. In this case, the solution temperature increases mainly due to Joule heating. The Joule heating can increase the solution temperature much faster than dielectric heating can. Also, the Joule heating is stronger near the high-voltage electrode since the electric potential at this location is the highest.[29] The Joule heating leads to local vaporization of the liquid to form small gas bubbles near the electrode. On the other hand, the presence of gas bubbles and increased solution temperature will reduce the dielectric strength of the solution and, in turn, lower the breakdown voltage.[46–48] The combined effect will allow the dielectric breakdown to occur at a voltage that is insufficient for a pure solvent. When the breakdown occurs, the electron emission and ionization (*i.e.*, the plasma formation) will further increase conductivity and lower the electrical resistance of the solution. As a result, the Joule heating effect will start to decrease when the plasma effect increases. Although some plasma species have high-energy densities and elevated temperatures, their thermal effect is much lower than the Joule heating effect. Thus, the balance between the Joule heating effect and the thermal effect due to the dispersion of the plasma species in the solution allows the solution temperature to stabilize

during a prolonged reaction time instead of continuously increasing.

Although adding small amounts of acid can reduce the breakdown voltage and facilitate the increase of the solution temperature, using higher acid concentrations causes a fall in the rate of temperature increase. This fall occurs because Joule heating effect becomes weaker with an increasing acid concentration in the solvent due to the decreased electrical resistance. On the other hand, supplying a higher voltage promotes Joule heating so that the solution temperature increases faster, and the breakdown can also be achieved more readily.

As shown above, sulfolane had a lower breakdown voltage than GVL, which is due to the different polarities of the two solvents. The dielectric breakdown in a solution is affected by the dielectric property of the solution, and this dielectric property of a solvent is directly related to its polarity. Usually, the more polar a solvent is, the higher its dielectric constant will be. A material with a high dielectric constant breaks down more easily than a material with a low dielectric constant. GVL has a polarity parameter (δ_P) of 12.1 whereas sulfolane has a δ_P of 18.2 (both at room temperature).[49] Therefore, the breakdown voltage was lower with sulfolane than GVL. The temperature increase was slightly lower in the sulfolane solutions due to the lower applied voltages and acid concentrations in the solution.

The theory above suggests that the increase of the solution temperature could affect cellulose conversion both directly and indirectly during plasma electrolysis. In our study, plasma electrolysis of cellulose was also performed in GVL with 7 mM of acid using a reactor placed in a 50 °C water bath to illustrate the decoupling of the temperature and plasma effect. As a result, the voltage of 6 kV was no longer sufficient to form a plasma in the same solution. Without plasma formation, cellulose remained mostly unconverted, and the LGO yield was merely 0.8% after a 20 min reaction (Table 3). When the water-bath was used to prevent the increase of the reactor temperature, the voltage had to be increased to 10 kV to achieve a breakdown in the GVL solution. Also, even with 10 kV voltage, the LGO yield only reached 9.4% after 20 min. As described above, the temperature of the GVL solution increased to nearly 160 °C with 6 kV voltage, and a 43.3% LGO yield was obtained after 15 min without the water-batch cooling of the reactor. Also, recall that the maximum LGO yield was 10.6% when cellulose was converted in the GVL solution at 160 °C by thermal heating. Thus, the results imply that coupled effects between the solution temperature and plasma formation present during plasma electrolysis of cellulose, which can synergistically enhance cellulose dissolution and LGO formation. Although the thermal effect of the increasing solution temperature alone does not significantly increase the reaction rate of cellulose conversion, a higher solution temperature was critical in improving cellulose dissolution and LGO formation. It enhances the conversion process not only by lowering the breakdown threshold to produce plasma species in the solution but also by accelerating the reaction rates for cellulose decomposition and dehydration that involve the plasma species.

3.4.2. The electrical resistance of the reaction solution. The plasma electrolysis involves electron emission and ionization, phenomena that are not expected to occur during conventional liquefaction in the solvents. If charged carriers are only produced during the plasma electrolysis, they will affect the electrical resistance of the solution. Thus, the solution resistances measured during the cellulose conversions in GVL with 7 mM of acid using both the plasma electrolysis and the thermal methods are compared in Fig. 5(a) as a function of the increasing solution temperature. Usually, the electric resistance of a substance is inversely correlated to the temperature of the substance. Consistent with this principle, decreases in the solution resistance were observed during conversion *via* either method. However, the resistance reduced significantly faster during plasma electrolysis. At 160 °C, the solution resistance was 0.32 MΩ with the thermal method, whereas it was only 0.03 MΩ with the plasma electrolysis. The decreasing resistance of the solution during the plasma electrolysis also

Table 3 Effect of solution temperature on LGO yield during plasma electrolysis in GVL with 7 mM acid. The frequency remains as 6 kHz

Solution temperature	Voltage	Plasma	Time [min]	LGO yield [%]
No-water bath (up to 160 °C)	6 kV	Yes	15	43.3
Water bath at 50 °C	6 kV	No	20	0.8
Water bath at 50 °C	10 kV	Yes	20	9.4

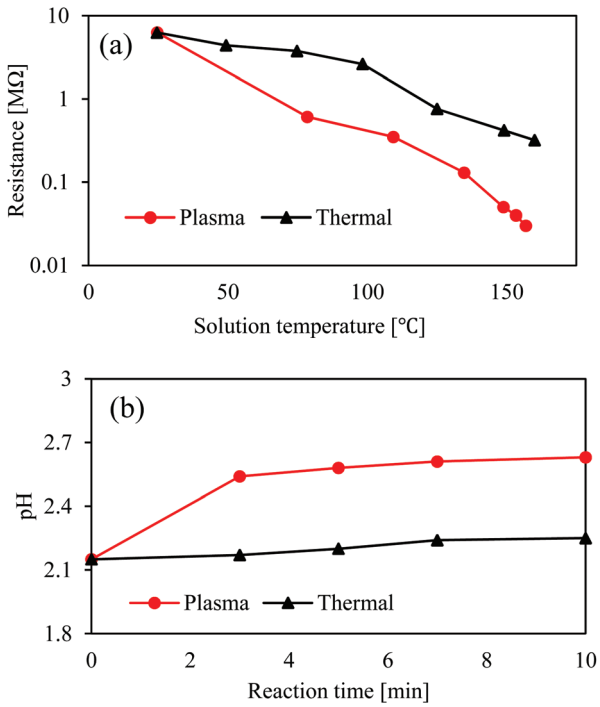

Fig. 5 Comparison of (a) electrical resistance and (b) pH value of reaction solution during cellulose conversions in GVL by plasma electrolysis and by the thermal heating method. Reaction conditions for the plasma electrolysis: 7 mM acid, V = 6 kV and f = 6 Hz.

corresponds to the increasing mobility of the particles in the solution for interactions.

3.4.3 Acid effect and solvent pH. During the plasma electrolysis, acid acts as more than just a catalyst. As described above, the acid ions in the dielectric solvent could promote the Joule heating to increase the solution temperature and therefore lower the breakdown voltage. Applying a high electric field to a diluted acidic solution can introduce the Wien effect to enhance ion mobility and promote interactions between cellulose and the ions. The fate of the H^+ ions was further investigated by measuring the solution pH during cellulose conversions in the GVL with 7 mM of acid *via* both the plasma electrolysis and the thermal methods. The results are compared in Fig. 5. During the plasma electrolysis, the solution pH increased from 2.15 to 2.54 within the first 3 min and then continually increased to 2.63 after a 10 min reaction. In comparison, there was only a minimal change in the solution pH when cellulose was converted using the thermal method. To further confirm this changing trend, the plasma electrolysis was also performed in GVL at other acid concentrations, and the pH of the solutions before and after the conversions were compared in Fig. S4.† As a result, the increase of the solution pH after the plasma electrolysis was observed for other acid concentrations as well. The highest pH increase occurred with 7 mM of acid, which is also the optimum solution condition for producing the highest LGO yield. The increased solution pH implies that the H^+ ions of the acid were consumed during the plasma electrolysis as they transformed into non-ionic species, for example, hydrogen radicals.

3.4.4. Radical formations. The dielectric breakdown under a high electric field creates a chemically rich environment that consists of electrons, ions, radicals, as well as excited atoms and molecules. The light-weight species released during the reactions were investigated by using OES to measure the surface of the solution during the plasma electrolysis of cellulose in GVL with 7 mM of acid. From the absorbance spectrum shown in Fig. 6, H radicals that are produced during the conversion could be identified.

Since neither hydrogen gas nor hydrogen donor agents were provided, the H radicals must be *in situ* generated in an unconventional way. There are three potential pathways for forming H radicals during the plasma electrolysis. In the first pathway, cellulose dehydration produces water, and water is further dissociated to form H and OH radicals (eqn (1)). In the second pathway, the H^+ ions in the solution accept free electrons emitted by the plasma discharge to become H radicals (eqn (2)).

$$H_2O \rightarrow 2H^{\bullet} + OH^{\bullet} \quad (1)$$

$$H^+ + e \rightarrow H^{\bullet} \quad (2)$$

Since the conversion to H radicals would reduce the concentration of H^+ ions, the observation of the increase of the solution pH described above can support this pathway. In the third pathway, hydrogen radicals are abstracted from glycosidic rings of cellulose, which will be discussed further in the later section. The formation of hydrogen radicals could also explain the presence of hydrogenated compounds among the products, such as 2-methyl furan, 1,3-butanediol, and 2-butene. These compounds were not found when cellulose was converted using the thermal method.

The presence of radicals in the reaction solution was also analyzed using EPR. In the EPR spectrum given in Fig. 7, a peak appearing at 3499 had the *G*-value of 2.0015. The peak was rather broad, suggesting that it could originate from a group of radicals rather than a single radical.[23,50] Previously, we reported that gas-phase plasma-treated cellulose generates a group of glycosidic radicals that have a lump *G*-value of 2.0089. Since the *G* value is different, it is unlikely that the radicals formed in this study are the same as the glycosidic radicals. In this study, the role of the radicals was investigated by adding spin trapping agents (PBN or DMPO) to the GVL solution and further converting cellulose using both plasma electrolysis and the thermal method. Adding the trapping agents did not affect the increase in the solution temperature or the dielectric breakdown. However, it strongly suppressed cellulose conversion in the solvent. As shown in Fig. S5,† cellulose barely dissolved or formed LGO. The solutions remained clear even after a 10 min reaction regardless of the type of trapping agent used. In comparison, there was no difference in the cellulose dissolution or LGO yield when the trapping agents were

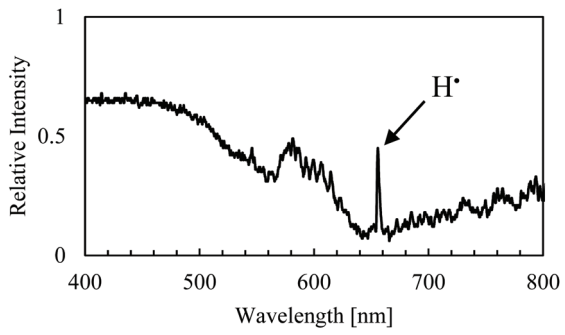

Fig. 6 OES spectrum obtained during plasma electrolysis of cellulose in GVL. Reaction conditions: V = 6 kV, f = 6 kHz and 7.0 mM acid.

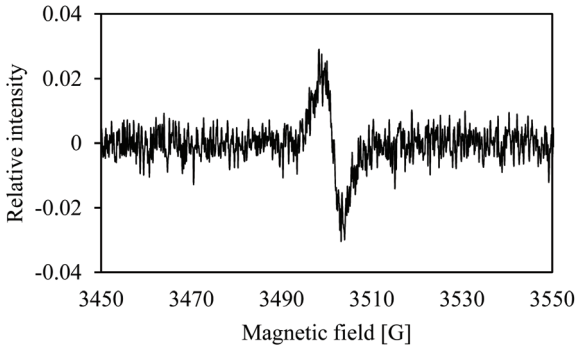

Fig. 7 EPR spectrum of the liquid product obtained from plasma electrolysis of cellulose in GVL. Reaction conditions: V = 6 kV, f = 6 kHz, 7 mM acid and 10 min reaction.

added during the thermal-based conversion of cellulose. The trapping agents react covalently with reactive radicals to form stable adducts. Terminating or deactivating the radicals dramatically suppressed cellulose conversion, which indicates that cellulose is mainly converted through a radical-based mechanism during plasma electrolysis. The radical formation under the plasma effect is critical in cellulose dissolution and monomer formation. The thermal-based conversion was not affected by the trapping agents since the conventional mechanism of cellulose conversion in the solvents does not proceed through a radical mechanism.

3.4.5. Proposed reaction mechanisms of cellulose by the plasma electrolysis. According to the conventional mechanism of cellulose decomposition, the cleavage of the glycosidic bond between two glucose units and a simultaneous C1–O–C6 bridging (*i.e.*, the concerted mechanism) produce LG and anhydro-oligosaccharides.[31,32,51–54] In the following steps, acid-catalyzed dehydration of LG leads to LGO as the major product with HMF and FF as the minor products.[37,38,55,56]

According to the conventional mechanism described above, LG is the major precursor of LGO. However, LG either was not observed or was produced in a minute quantity during the plasma electrolysis of cellulose. On the other hand, a significant amount of DGP was formed during the plasma electrolysis, and it always reached the optimal yield point earlier than LGO did in the same solution. Hence, cellulose could have been converted to DGP first and then subsequently dehydrated to LGO. Also, recall that radical formation during the plasma electrolysis was directly related to cellulose dissolution. Since cellulose dissolution is usually due to decrystalization and the decrease in chain length,[57–59] radicals must form during the cellulose chain deconstruction. While homolytic cleavage of the glycosidic linkage is the most plausible method for forming radicals, the plasma-induced hydrogen abstractions at the glycosidic-rings can also lead to hydroxyalkyl radicals in cellulose.[60]

The proposed radical-based mechanism of forming DGP as a precursor of LGO is illustrated in Fig. 8. When the glycosidic

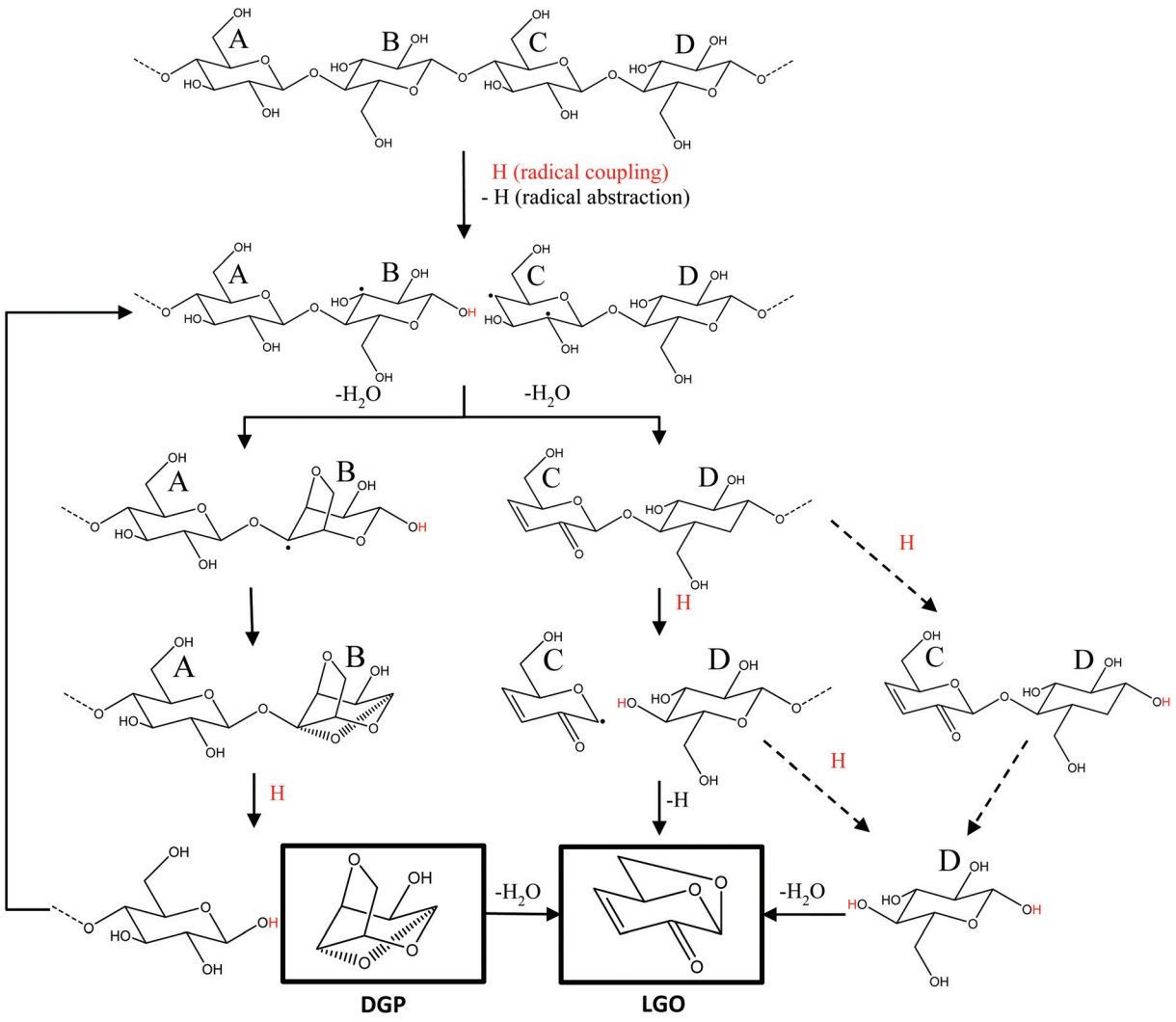

Fig. 8 Proposed reaction mechanisms of cellulose during plasma electrolysis.

bond between the glucose unit A and B cleaves, a hydrogen radical generated *in situ* during the plasma electrolysis combines with the glycosidic radical C1–O through a hydrogen radical coupling to form a reducing end in unit B. In the subsequent reaction, dehydration between the hydroxyalkyl radical at C3 (due to a hydrogen abstraction) and the hydroxyl at C6 leads to a C3–O–C6 bridge and the formation of an alkoxyalkyl radical at C4. The alkoxyalkyl radical further attacks the hydroxyl group at C1 in the same unit to form a C1–O–C4 bridge. During this bridging, the glycosidic bond between unit A and C is cleaved, resulting in a DGP molecule originated from unit B and a C1–O radical in unit A. The subsequent hydrogen radical coupling at the C1–O radical produces a reducing end in unit A. By repeating the abovementioned process, more DGP molecules can be produced, which is subsequently dehydrated to form LGO. Since this radical depropagation process enables both the chain depolymerization and the ring dehydration at the same time, cellulose dissolution and LGO formation are both enhanced during the plasma electrolysis.

Other than the abovementioned pathway, LGO can also be produced directly from unit C. As also shown in Fig. 8, the radical at C4 in unit C is the result of the glycosidic bond cleavage between the unit B and C, and the hydroxyalkyl radical at C2 is due to a hydrogen abstraction from the glycosidic ring. Facile dehydration involving the hydroxyalkyl radical and the hydroxyl at C3 can lead to a carbonyl bond at C2 and an arylalkyl radical at C3. The radicals at C3 and C4 are then stabilized through the formation of a carbon–carbon double bond in the ring. On the other hand, the homolytic cleavage at the glycosidic bond between the units C and D forms a radical at C1 of unit C. The interaction between the C1 radical and the hydroxyl at C6 in the same unit leads to an LGO molecule and a free hydrogen radical. On another side, a hydrogen radical coupling at the C4–O radical of unit D can produce a reducing end. If the glycosidic ring cleavage followed by a radical coupling occurs between unit D and its neighboring unit on another side, a dimer that is the combination of a glucose and an LGO molecule could be formed. In fact, such a dimer structure was identified by the GC/MS analysis of the liquid product, which supports our theory. According to the proposed mechanisms, glucose can also be produced as a result of the hydrogen radical coupling.

In the proposed radical mechanisms, the formation of reducing ends *via* hydrogen radical coupling plays a critical role in enabling the radical-based depropagation reactions. Without hydrogen radicals, a non-reducing end (or an LG end) would be produced. Therefore, the effect of the hydrogen radical coupling on the formation of the reducing ends was investigated by comparing the plasma electrolysis of glucose and LG both in GVL with 7 mM of acid. The yields of LGO and DGP from glucose were 24.5 and 8.5%, respectively, compared to 2.5% and 5.2% with LG (Table S1†). During the plasma electrolysis, LG produced FF more selectively. Therefore, the result supports the proposed role of hydrogen radicals. The hydrogen radical coupling also explains why cellulose conversion could be enhanced despite the fact that the concentration of hydrogen ions in the solution decreased during the course of plasma electrolysis. Generating a higher amount of hydrogen radicals would be beneficial to the formation of more reducing ends and therefore promotes more effective depropagation.

4. Conclusions

In this study, we produced LGO and other biobased chemicals based on plasma electrolysis of cellulose in polar aprotic solvents without the use of external heating. Based on side-by-side comparison experiments performed in this study using the same amounts of cellulose in the same volumes of the solutions, plasma electrolysis was able to produce a 154% higher LGO yield using 28% of the energy consumed by using the thermal-based method when the conversions were carried out in GVL solutions. In the case sulfolane was the conversion solvent, plasma electrolysis produced a 28% higher LGO yield from cellulose using only 3% of the energy consumed during the thermal-based conversion. Our analyses suggest that hydrogen radical coupling and radical-based depropagation are critical in achieving complete solubilization of cellulose and effective production of LGO. During the plasma electrolysis, synergistic effects between Joule heating and plasma chemistry could lower the breakdown conditions and increase reaction rates. The present study suggests that by selecting solvent systems and tuning the experimental variables, biobased chemicals can be produced more effectively using the plasma electrolysis process. In future studies, energy saving advantages of plasma electrolysis compared to other conversion technologies should be systemically evaluated by performing detailed energy balances.

Conflicts of interest

There are no conflicts to declare.

Acknowledgements

The authors would like to acknowledge Dr Sarah Cady from the Department of Chemistry at Iowa State University for providing technical support in the EPR analyses. The authors also acknowledge the instrument support from Bioeconomy Institute at Iowa State University.

References

1 F. H. Isikgor and C. R. Becer, *Polym. Chem.*, 2015, **6**, 4497–4559.
2 S. Choi, C. W. Song, J. H. Shin and S. Y. Lee, *Metab. Eng.*, 2015, **28**, 223–239.

3 S. H. Krishna, K. Huang, K. J. Barnett, J. He, C. T. Maravelias, J. A. Dumesic, G. W. Huber, M. De bruyn and B. M. Weckhuysen, *AIChE J.*, 2018, **64**, 1910–1922.
4 Z. Jiang, P. Zhao and C. Hu, *Bioresour. Technol.*, 2018, **256**, 466–477.
5 Z. Zhang and G. W. Huber, *Chem. Soc. Rev.*, 2018, **47**, 1351–1390.
6 K. Weltmann, J. F. Kolb, M. Holub, D. Uhrlandt, M. Šimek, K. (Ken) Ostrikov, S. Hamaguchi, U. Cvelbar, M. Černák, B. Locke, A. Fridman, P. Favia and K. Becker, *Plasma Processes Polym.*, 2019, **16**, 1800118.
7 J. Vanneste, T. Ennaert, A. Vanhulsel and B. Sels, *ChemSusChem*, 2017, **10**, 14–31.
8 Y. Fan, W. Zhao, S. Shao, Y. Cai, Y. Chen and L. Jin, *Energy*, 2018, **142**, 462–472.
9 Y. Fan, Y. Xiong, L. Zhu, L. Fan, L. Jin, Y. Chen and W. Zhao, *Chem. Eng. Process.*, 2019, **135**, 53–62.
10 H. Taghvaei and M. R. Rahimpour, *Process Saf. Environ. Prot.*, 2019, **121**, 221–228.
11 X. Liu, T. He, Y. Ge, G. Li, J. Wu, Z. Wang, G. Liu and J. Wu, *J. Anal. Appl. Pyrolysis*, 2018, **131**, 128–133.
12 A. Wright, H. Bandulasena, C. Ibenegbu, D. Leak, T. Holmes, W. Zimmerman, A. Shaw and F. Iza, *AIChE J.*, 2018, **64**, 3803–3816.
13 M. Lim and A. Z. S. Zulkifli, *Plasma Sci. Technol.*, 2018, **20**, 115502.
14 D. L. Tsyganov, N. Bundaleska and E. Tatarova, *Plasma Processes Polym.*, 2017, **14**, 1600161.
15 F. Jérôme, *Curr. Opin. Green Sustainable Chem.*, 2016, **2**, 10–14.
16 R. Nastase, E. Fourré, M. Fanuel, X. Falourd and I. Capron, *Carbohydr. Polym.*, 2020, **231**, 115704.
17 N. Bundaleska, E. Tatarova, F. M. Dias, M. Lino da Silva, C. M. Ferreira and J. Amorim, *J. Phys. D: Appl. Phys.*, 2014, **47**, 055201.
18 A. I. Maksimov and A. Y. Nikiforov, *High Energy Chem.*, 2007, **41**, 454–459.
19 J. Gao, L. Chen, J. Zhang and Z. Yan, *Bioresour. Technol.*, 2014, **171**, 469–471.
20 M. Boutonnet Kizling and S. G. Järås, *Appl. Catal., A*, 1996, **147**, 1–21.
21 W. Zhao, J. Huang, K. Ni, X. Zhang, Z. Lai, Y. Cai and X. Li, *J. Energy Inst.*, 2018, **91**, 595–604.
22 L. Di, J. Zhang and X. Zhang, *Plasma Processes Polym.*, 2018, **15**, 1700234.
23 L. A. H. Hu and X. Bai, *Green Chem.*, 2020, **22**, 2036–2048.
24 I. Prasertsung, P. Chutinate, A. Watthanaphanit, N. Saito and S. Damrongsakkul, *Carbohydr. Polym.*, 2017, **172**, 230–236.
25 O. Takai, *J. Photopolym. Sci. Technol.*, 2014, **27**, 379–384.
26 I. Prasertsung, K. Aroonraj, K. Kamwilaisak, N. Saito and S. Damrongsakkul, *Carbohydr. Polym.*, 2019, **205**, 472–479.
27 D. Tang, X. Zhang and S. Yang, *Plasma Sci. Technol.*, 2018, **20**, 044002.
28 D. Xi, C. Jiang, R. Zhou, Z. Fang, X. Zhang, Y. Liu, B. Luan, Z. Feng, G. Chen, Z. Chen, Q. Liu and S. Yang, *Bioresour. Technol.*, 2018, **268**, 531–538.
29 C.-C. Jiang, S.-Y. Liu, Z. Feng, Z. Fang, X.-H. Zhang, D.-H. Mei, D.-K. Xi, B.-Y. Luan, X.-Q. Wang and S.-Z. Yang, *Chin. Phys. B*, 2019, **28**, 048803.
30 S. Wu, S. Deng, J. Zhu, M. A. Bashir and F. Izuno, *J. Cleaner Prod.*, 2019, **228**, 405–417.
31 F. Cao, T. J. Schwartz, D. J. McClelland, S. H. Krishna, J. A. Dumesic and G. W. Huber, *Energy Environ. Sci.*, 2015, **8**, 1808–1815.
32 J. He, M. Liu, K. Huang, T. W. Walker, C. T. Maravelias, J. A. Dumesic and G. W. Huber, *Green Chem.*, 2017, **19**, 3642–3653.
33 G. Dobele, G. Rossinskaja, G. Telysheva, D. Meier, S. Radtke and O. Faix, in *Progress in Thermochemical Biomass Conversion*, Blackwell Science Ltd, Oxford, UK, 2008, pp. 1500–1508.
34 M. B. Comba, Y. Tsai, A. M. Sarotti, M. I. Mangione, A. G. Suárez and R. A. Spanevello, *Eur. J. Org. Chem.*, 2018, **2018**, 590–604.
35 F. Shafizadeh, R. H. Furneaux and T. T. Stevenson, *Carbohydr. Res.*, 1979, **71**, 169–191.
36 X. Ye, Q. Lu, X. Wang, H. Guo, M. Cui, C. Dong and Y. Yang, *ACS Sustainable Chem. Eng.*, 2017, **5**, 10815–10825.
37 Z. Zhang, Q. Lu, X. Ye, T. Wang, X. Wang and C. Dong, *BioEnergy Res.*, 2015, **8**, 1263–1274.
38 S. Kudo, N. Goto, J. Sperry, K. Norinaga and J.-I. Hayashi, *ACS Sustainable Chem. Eng.*, 2017, **5**, 1132–1140.
39 A. Ghosh, X. Bai and R. C. Brown, *ChemistrySelect*, 2018, **3**, 4777–4785.
40 J. S. Luterbacher, J. M. Rand, D. M. Alonso, J. Han, J. T. Youngquist, C. T. Maravelias, B. F. Pfleger and J. A. Dumesic, *Science*, 2014, **343**, 277–280.
41 H. Kawamoto, S. Saito, W. Hatanaka and S. Saka, *J. Wood Sci.*, 2007, **53**, 127–133.
42 K. Wang, J. Ye, M. Zhou, P. Liu, X. Liang, J. Xu and J. Jiang, *Cellulose*, 2017, **24**, 1383–1394.
43 A. Ghosh, R. C. Brown and X. Bai, *Green Chem.*, 2016, **18**, 1023–1031.
44 H. Kawamoto, W. Hatanaka and S. Saka, *J. Anal. Appl. Pyrolysis*, 2003, **70**, 303–313.
45 D. M. Alonso, S. G. Wettstein and J. A. Dumesic, *Green Chem.*, 2013, **15**, 584.
46 P. Bruggeman, D. Schram, M. Á. González, R. Rego, M. G. Kong and C. Leys, *Plasma Sources Sci. Technol.*, 2009, **18**, 025017.
47 P. Bruggeman and C. Leys, *J. Phys. D: Appl. Phys.*, 2009, **42**, 053001.
48 H. Yui, Y. Someya, Y. Kusama, K. Kanno and M. Banno, *J. Appl. Phys.*, 2018, **124**, 103301.
49 C. M. Hansen, *Hansen Solubility Parameters*, CRC Press, 2007.
50 K. H. Kim, X. Bai, S. Cady, P. Gable and R. C. Brown, *ChemSusChem*, 2015, **8**, 894–900.
51 R. Weingarten, A. Rodriguez-Beuerman, F. Cao, J. S. Luterbacher, D. M. Alonso, J. A. Dumesic and G. W. Huber, *ChemCatChem*, 2014, **6**, 2229–2234.
52 H. B. Mayes and L. J. Broadbelt, *J. Phys. Chem. A*, 2012, **116**, 7098–7106.

53 T. Hosoya and S. Sakaki, *ChemSusChem*, 2013, **6**, 2356–2368.
54 W. Wan, L.-J. Yu and A. Karton, *Aust. J. Chem.*, 2016, **69**, 943.
55 B. Hu, Q. Lu, Y. Wu, W. Xie, M. Cui, J. Liu, C. Dong and Y. Yang, *J. Energy Chem.*, 2020, **43**, 78–89.
56 O. Oyola-Rivera, J. He, G. W. Huber, J. A. Dumesic and N. Cardona-Martínez, *Green Chem.*, 2019, **21**, 4988–4999.
57 R. C. Saxena, D. K. Adhikari and H. B. Goyal, *Renewable Sustainable Energy Rev.*, 2009, **13**, 167–178.
58 D. Ciolacu, F. Ciolacu and V. I. Popa, *Cellul. Chem. Technol.*, 2011, **45**, 13–21.
59 D. Klemm, B. Heublein, H.-P. Fink and A. Bohn, *Angew. Chem., Int. Ed.*, 2005, **44**, 3358–3393.
60 M. Kuzuya and Y. Yamauchi, *Thin Solid Films*, 1998, **316**, 158–164.